Local density of states of ⟨110⟩-split interstitials and their neighbors in molybdenum

J. A. Blah, S. S. Pohlong, and P. N. Ram
Department of Physics, North-Eastern Hill University, Shillong 793003, Meghalaya, India
(Received 25 May 1993; revised manuscript received 1 November 1993)

In a previous paper we studied the dynamics of self-interstitial atoms in bcc metals and calculated the local density of states of the ⟨110⟩ dumbbell in Mo using a Green's-function method. In this paper, we calculate the local density of states of neighbors of the dumbbell which affect the properties of the irradiated metal significantly. The local density of states of the neighbors show the same well-known resonance and localized modes shown by the dumbbell spectrum. However, the amplitude of vibrations of neighbors in the resonant modes is, in general, very small so that only the spectrum of the closest neighbor in the $(1\bar{1}0)$ plane shows clearly all the resonant modes found with the dumbbell spectrum. The result is discussed in the light of Mössbauer measurements of irradiated *Mo* ^{57}Co. Contrary to earlier expectations, the vibrational modes of the Mössbauer atom located at a substitutional site nearest to a dumbbell atom do not explain the observed reduction in the Debye-Waller factor.

I. INTRODUCTION

In most of the studies of self-interstitial atoms (SIA's) in metals, the focus of attention has been the fcc metals[1–12] and, in comparison, less attention has been paid to bcc metals: though the symmetry and structure of SIA's have been investigated by computer simulation and the ⟨110⟩-dumbbell configuration, at least in α-Fe, Mo, and W, has been found,[13] studies on the dynamics of this defect are still lacking. In a detailed investigation of irradiated *Mo* ^{57}Co Marangos, Mansel, and Vogl[14] have identified different sites for single- and di-interstitials trapped at the ^{57}Co atom. It is proposed that a ⟨110⟩ self-interstitial is trapped at a ^{57}Co atom on a substitutional lattice site (Fig. 1) and that this configuration is unstable on annealing above 125 K. Further, to study the dynamical behavior of trapped interstitials, Marangos, Mansel, and Wahl[15] measured the temperature dependence of the Mössbauer spectra before irradiation and after post-irradiation annealing at 124 K and found a large reduction in the Debye-Waller factor. These authors explained the measurements by invoking a resonant mode at $0.1\omega_{max}$ and a localized mode just above ω_{max} for the defect complex, and believe that the low-frequency mode should correspond essentially to the resonant mode of the ⟨110⟩-split interstitial in Mo. However, a strong reduction in the Debye-Waller factor with increasing temperature has to be attributed to a strong shift of the density of states of the Mössbauer impurity to lower frequencies.

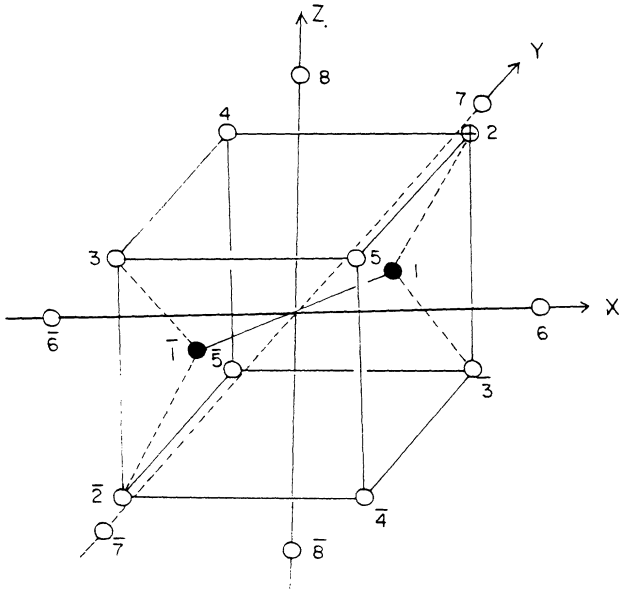

FIG. 1. ⟨110⟩-dumbbell configuration in the bcc lattice showing the defect space. ○, host atom; ●, dumbbell atom; and ⊕ the nearest neighbor to be substituted by the Mössbauer impurity ^{57}Co.

Recently one of us (P.N.R.) reported a calculation of the local density of states of the ⟨110⟩ dumbbell in Mo.[16] As might be expected, many of the characteristics of the behavior of SIA's in fcc metals are also exhibited by SIA's in bcc metals: the ⟨110⟩-dumbbell spectrum shows a number of low-frequency resonant modes and high-frequency localized modes, and the resonance modes lead to much-enhanced thermal displacements of the defect, and can explain the large reduction in shear moduli and provide a consistent picture of long-range migration of SIA's in Mo. The result of enhanced thermal displacements was seen to be consistent with the Mössbauer study of trapped interstitials at ^{57}Co by Marangos, Mansel, and Wahl.[15] However, it was felt that for a detailed comparison with experiment the appropriate quantity is the square of the thermal displacement of one of the neighbors of the dumbbell in the $(1\bar{1}0)$ plane which is supposed to be substituted by the Mössbauer impurity (Fig. 1). Though in a resonant mode the motion of the neighbor is in phase with that of the dumbbell atom and thus the same resonance is involved in the vibration of the dumbbell as well as the neighboring ^{57}Co atom, the observed strong reduction in the Debye-Waller factor has to be explained with the use of the local density of states of the neighbor, which is expected to show possible reso-

nant modes contributing to the vibrational behavior of the concerned atom. This is one of the reasons for the present study.

Following our earlier work we have calculated the local density of states of not only the dumbbell atom but also its neighboring atoms falling in the cluster of first and second neighbors of the defect site. Apart from the well-known resonant and localized modes seen in the local density of states of the dumbbell atom, the local densities of states of the close neighbors of the interstitial do not show any additional resonant or localized modes. The amplitudes of vibrations of the neighbors are much smaller than those of the dumbbell atom so that the intensity of the resonant modes is much reduced in the case of the neighbor-atom spectra. As a matter of fact, the frequency spectrum of atom 4 (Fig. 1), a nearest-neighbor atom in the (110) plane, barely shows resonant structures while the spectrum of atom 8, the next-nearest neighbor on the z axis, does not show resonant structure at all. Though the frequency spectrum of the closest neighbor in the $(1\bar{1}0)$ plane (atom 2) shows all the resonant modes, their intensities are much reduced. The spectrum shifts equally to low- and high-frequency regions giving, respectively, resonant and localized modes. However, because of the reduced intensity of resonant modes the calculated mean-square displacement of atom 2 shows only a slight increase over the mean-square displacement of a host atom. This result is contrary to earlier expectations[15,16] that the spectrum of atom 2 would be shifted to the low-frequency region, resulting in a large increase in the mean-square displacement and consequently a large reduction in the Debye-Waller factor.

II. THEORY

If we consider the same-site Green's function, the total density of states of the lattice can be expressed as the sum of the imaginary parts of the lattice Green's function over all the lattice sites,

$$Z(\omega)=\frac{2\omega M}{\pi}\sum_{l,\alpha}\mathrm{Im}G_{\alpha\alpha}(l,l;\omega)\ , \tag{1}$$

where a monatomic lattice is considered. Here, l represents the lattice site and α the Cartesian coordinates. We define the local density of states of atom l in the α direction as[1,3]

$$Z_\alpha(l,\omega)=\frac{2\omega M}{\pi}\mathrm{Im}G_{\alpha\alpha}(l,l;\omega)\ . \tag{2}$$

If we write the Green's function in terms of the eigenvectors $U(l,s)$ of the dynamical matrix of the lattice, then the expression for the local density of states for site l will transform to

$$Z_\alpha(l,\omega)=\sum_s |U_\alpha(l,s)|^2\delta(\omega_s-\omega),\quad \omega>0\ , \tag{3}$$

with

$$\int_0^\infty d\omega\, Z_\alpha(l,\omega)=\sum_s |U_\alpha(l,s)|^2=1\ . \tag{4}$$

Obviously, the total density of states of the lattice can be expressed as the sum of the local density of states of all the atoms in all three directions,

$$Z(\omega)=\sum_{l,\alpha} Z_\alpha(l,\omega)\ . \tag{5}$$

In order to obtain the local density of states we use a defect model with second-nearest-neighbor interactions. The defect model to be used has been described previously.[16,17] The defect space for the $\langle 110\rangle$-dumbbell configuration is shown in Fig. 1. The defect is described by an assumed vacancy at the origin and interstitial atoms at $(\pm x,\pm x,0)a/2$, where a is the lattice constant. In this model the dumbbell is surrounded by eight nearest neighbors and six second-nearest neighbors, and as such the defect space consists of 17 sites and one has to deal with 51×51 matrices. In order to reduce the complexity of the calculation, group theory is used to decompose the defect space into various irreducible representations. For the dumbbell atom the defect Green's function is

$$\begin{aligned}G_{XX}(d,d;\omega)&=G_{YY}(d,d;\omega)\\&=\tfrac{1}{4}[G_{CC}(A_g)+G_{CC}(B_{1g})\\&\quad+G_{CC}(B_{2u})+G_{CC}(B_{3u})]\end{aligned} \tag{6a}$$

and

$$G_{ZZ}(d,d;\omega)=\tfrac{1}{2}[G_{CC}(B_{2g})+G_{CC}(B_{1u})]\ , \tag{6b}$$

where $G_{CC}(\omega)=(\phi_{CC}-\phi_{CR}\hat{G}_{RR}(\omega)\phi_{RC}-M_{CC}\omega^2)^{-1}$ describes the local vibrational properties of the interstitial whose poles (quasipoles) determine the frequencies of localized (resonant) modes. Here, ϕ_{CC} is the Einstein force constant for the interstitial space while ϕ_{CR} or ϕ_{RC} describes the coupling of the interstitial with the neighbors; the Green's function $\hat{G}_{RR}$ refers to the host space when the interstitial is fixed. The Green's functions for the neighboring atoms are found to be

$$\begin{aligned}G_{XX}(2,2;\omega)&=G_{YY}(2,2;\omega)\\&=\tfrac{1}{8}[G^{11}_{RR}(A_g)+G^{11}_{RR}(B_{1g})+G^{11}_{RR}(B_{2g})\\&\quad+G^{11}_{RR}(B_{3g})+G^{11}_{RR}(A_u)+G^{22}_{RR}(B_{1u})\\&\quad+G^{22}_{RR}(B_{2u})+G^{22}_{RR}(B_{3u})]\ ,\end{aligned} \tag{7a}$$

$$\begin{aligned}G_{ZZ}(2,2;\omega)&=\tfrac{1}{4}[G^{22}_{RR}(A_g)+G^{22}_{RR}(B_{2g})\\&\quad+G^{33}_{RR}(B_{1u})+G^{33}_{RR}(B_{3u})]\ ,\end{aligned} \tag{7b}$$

$$\begin{aligned}G_{XX}(4,4;\omega)&=G_{YY}(4,4;\omega)\\&=\tfrac{1}{8}[G^{33}_{RR}(A_g)+G^{22}_{RR}(B_{1g})+G^{33}_{RR}(B_{2g})\\&\quad+G^{22}_{RR}(B_{3g})+G^{22}_{RR}(A_u)+G^{44}_{RR}(B_{1u})\\&\quad+G^{33}_{RR}(B_{2u})+G^{44}_{RR}(B_{3u})]\ ,\end{aligned} \tag{8a}$$

$$\begin{aligned}G_{ZZ}(4,4;\omega)&=\tfrac{1}{4}[G^{44}_{RR}(A_g)+G^{33}_{RR}(B_{3g})\\&\quad+G^{55}_{RR}(B_{1u})+G^{44}_{RR}(B_{2u})]\ ,\end{aligned} \tag{8b}$$

$$G_{XX}(6,6;\omega)=\tfrac{1}{4}[G^{55}_{RR}(A_g)+G^{33}_{RR}(B_{1g}) +G^{55}_{RR}(B_{2u})+G^{55}_{RR}(B_{3u})]\ , \tag{9a}$$

$$G_{YY}(6,6;\omega)=\tfrac{1}{4}[G^{66}_{RR}(A_g)+G^{44}_{RR}(B_{1g}) +G^{66}_{RR}(B_{2u})+G^{66}_{RR}(B_{3u})]\ , \tag{9b}$$

$$G_{ZZ}(6,6;\omega)=\tfrac{1}{4}[G^{44}_{RR}(B_{2g})+G^{44}_{RR}(G_{3g}) +G^{33}_{RR}(A_u)+G^{66}_{RR}(B_{1u})]\ , \tag{9c}$$

$$G_{XX}(8,8;\omega)=G_{YY}(8,8;\omega) =\tfrac{1}{4}[G^{55}_{RR}(B_{2g})+G^{55}_{RR}(B_{3g}) +G^{77}_{RR}(B_{2u})+G^{77}_{RR}(B_{3u})]\ , \tag{10a}$$

$$G_{ZZ}(8,8;\omega)=\tfrac{1}{2}[G^{77}_{RR}(A_g)+G^{77}_{RR}(B_{1u})]\ , \tag{10b}$$

where the atoms are numbered according to Fig. 1 and where the Green's function $G_{RR}=[\phi_{RR}-\phi_{RC}\hat{G}_{CC}(\omega)\phi_{CR}-M_{RR}\omega^2]^{-1}$ gives the vibrations of the host lattice in the presence of the interstitial, while at the same time eliminating the additional degrees of freedom due to its presence. Here ϕ_{RR} represents the force constant in the host space when the interstitial is fixed, and the Green's function $\hat{G}_{CC}$ refers to the interstitial vibrations in a frozen lattice. The Green's function G_{RR} can also be expressed in terms of the perfect-lattice Green's function $\mathring{G}$ and the perturbation including the interstitial reaction to the lattice system,

$$G_{RR}=\mathring{G}(1+\tilde{v}_{RR}\mathring{G})^{-1}\ , \tag{11}$$

with

$$\tilde{v}_{RR}=\phi_{RR}-\mathring{\phi}-\phi_{RC}\hat{G}_{CC}\phi_{CR}\ ,$$

and, therefore, the condition for localized and resonance modes is given by

$$\mathrm{Re}\det(1+\tilde{v}_{RR}\mathring{G})=0\ . \tag{12}$$

This equation gives all possible localized and resonance modes including those in which the dumbbell atom is at rest. Now the local density of states of a particular atom is

$$Z(l,l;\omega)=\frac{2\omega M}{3\pi}\mathrm{Im}[G_{XX}(l,l;\omega)+G_{YY}(l,l;\omega) +G_{ZZ}(l,l;\omega)]\ . \tag{13}$$

From the elements of the Green's function for the dumbbell atom and its neighbors one can already see the displacement pattern of atoms in the defect space for various irreducible representations. This can also be inferred from the symmetry coordinates. The motion of the dumbbell atom and four of its closest neighbors in the $(1\bar{1}0)$ plane referring to various irreducible representations is indicated in Fig. 2. The displacement amplitudes shown in Fig. 2 in our earlier paper[16] for the B_{2g}, B_{1u}, and B_{3u} modes are in error and have now been corrected. As can be inferred from Fig. 2, except for irreducible representation A_g, where a more dominant longitudinal force constant between dumbbell atoms is involved, in all other irreducible representations the nature of the vibrational modes is controlled by transverse force constants and consequently the nature of the characteristic mode is determined by the phase shift between motions of the dumbbell atom and its neighbors: they are in phase in resonant modes and out of phase in localized modes. Not surprisingly, the local density of states of the dumbbell shows only localized modes pertaining to breathing modes (A_{1g} or A_g), whereas both localized and resonant modes are found for other modes.[1-3]

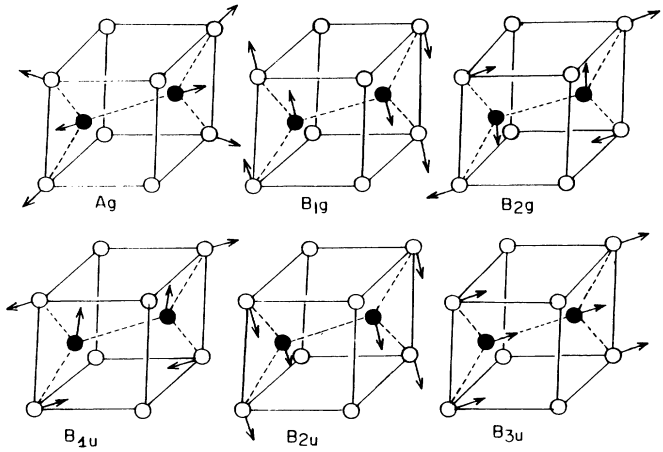

FIG. 2. Vibrational modes of the ⟨110⟩ dumbbell in the bcc lattice showing the vibrational amplitudes of the dumbbell atom and its nearest neighbors in the $(1\bar{1}0)$ plane: localized (A_g) and resonant modes.

III. NUMERICAL RESULTS AND DISCUSSION

In order to calculate the local density of states one has to generate the ideal-lattice Green's functions in addition to evaluating the force constants in the vicinity of the defect. To compute the perfect-lattice phonons to be used for the evaluation of lattice Green's functions, use has been made of the third-nearest-neighbor axially symmetric force model obtained from Born–von Karman fits to the measured phonons in neutron-scattering experiments.[18] For the calculation of Green's functions we follow a modified Gilat-Raubenheimer method.[19] We consider interaction between two atoms to be represented by the usual two force constants derived from the central potential $\phi(r)$, a longitudinal force constant $d^2\phi(r)/dr^2|_0$ and a transverse force constant $(1/r)(d\phi/dr)|_0$, where the suffix 0 indicates that the derivatives have to be evaluated at the equilibrium distance between the atoms. For the present defect model, we consider five sets of force constants corresponding to five different distances between the following pairs of atoms $(1,\bar{1})$, (1,2), (1,4), (1,6), and (1,8) (see Fig. 1). The vacancy is described by zero coupling to its neighbors. The equilibrium positions of various atoms in the defect space have been determined by the Green's-function method of lattice statics.[17] For calculating lattice distortion and various force constants in the defect space, we use the potential constructed by Johnson and Wilson (JW) from elastic constants and unrelaxed-vacancy formation energy.[20] The detailed pro-

cedure for evaluating the force constants as well as a justification for the use of the JW potential have been reported earlier.[16]

The calculated local densities of states of the dumbbell atom and its neighbors are plotted in Figs. 3–7. In these figures the host-lattice spectrum is also included for comparison. As found earlier, the frequency spectrum of the dumbbell (Fig. 3) shows six resonant modes and six localized modes. The frequencies of the resonant and localized modes are given in Table I.

As for the frequency spectra of the neighboring atoms (Figs. 4–7), the spectrum of atom 2 is remarkable in more than one way: atom 2 being one of the closest neighbors of the dumbbell, its vibrations are most strongly influenced by the defect; its vibrations in the $(1\bar{1}0)$ plane are expected to participate prominently in some of the resonant modes shown by the dumbbell spectrum. As can be seen from Fig. 4, all the resonance modes seen with the dumbbell spectrum are present in this spectrum as well but with much reduced intensity; there is significant reduction in the density of high-frequency modes, but unlike the dumbbell-atom spectrum there is no matching increase in the intensity in the low-frequency region. It is clear that part of the missing modes at higher frequencies must be accounted for by localized modes above the maximum frequency. A fairly clear idea about this behavior can be obtained if we compare the integrated densities of states of the dumbbell atom, atom 2, and a host atom up to the maximum frequency $\omega_{\max}$ as well as in the low-frequency region, e.g., up to $\omega_{\max}/2$. The calculated values are

$$\int_0^{\omega_{\max}} Z(d,\omega)d\omega = 0.6322 ,$$
$$\int_0^{\omega_{\max}/2} Z(d,\omega)d\omega = 0.500 ,$$
$$\int_0^{\omega_{\max}} Z(2,\omega)d\omega = 0.7144 ,$$
$$\int_0^{\omega_{\max}/2} Z(2,\omega)d\omega = 0.1940 ,$$

TABLE I. Frequencies (in THz) of resonance and localized modes.

Irreducible representation	Resonance mode ν_r [a]	Localized mode ν_l
A_g		8.26, 12.77
B_{1g}	1.39, 7.995	
B_{2g}	2.73	12.17
B_{1u}	3.55	12.38
B_{2u}	3.11	8.07
B_{3u}	2.59	10.965

[a]The frequencies of the B_{2u} and B_{1u} resonant modes reported in Ref. 16 are in error.

$$\int_0^{\omega_{\max}} \mathring{Z}(\omega)d\omega = 1.000 ,$$
$$\int_0^{\omega_{\max}/2} \mathring{Z}(\omega)d\omega = 0.0935 .$$

This shows that, while for the dumbbell atom the shift of the spectrum to the low-frequency region is quite significant, the spectrum of atom 2 shows no such shift to the lower frequencies. Though the dumbbell atom and atom 2 are involved in the same resonance modes, the amplitude of vibration of atom 2 is much smaller than that of the dumbbell atom, especially for the low-frequency resonant modes. Such a behavior for a resonant mode is not unexpected. In fact, quite generally in resonant modes the amplitude of vibration of an impurity is greatly enhanced compared to its neighbors. This has been explicitly demonstrated for a substitutional impurity in the linear-chain model.[21] In the analogous system of the ⟨100⟩ dumbbell in a fcc metal, Zeller[22] has estimated the relative amplitudes of the dumbbell atom and its neighbors for low-frequency resonant modes and has found that the amplitude of the neighbors is much smaller than that of the dumbbell atom.

Of the remaining neighbors for which frequency spec-

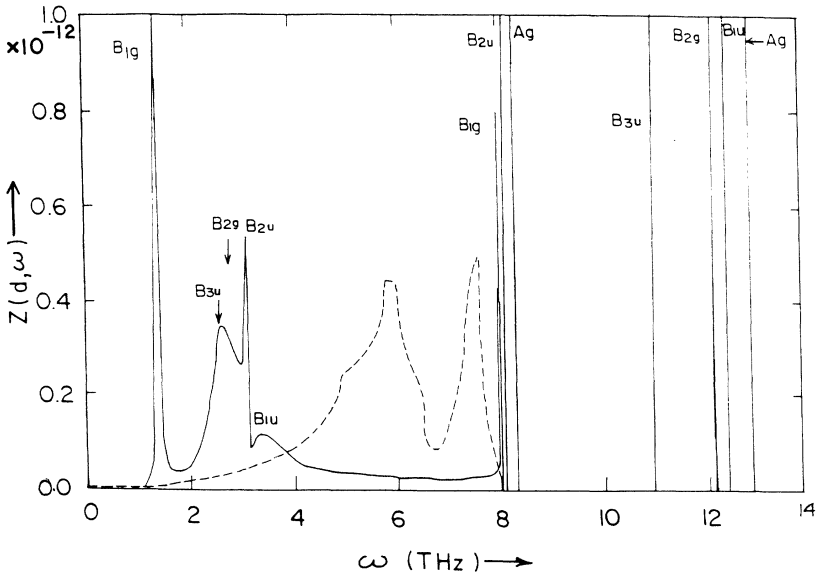

FIG. 3. Local density of vibrational states of the ⟨110⟩-dumbbell atom (——) and an atom in the host lattice (— — —).

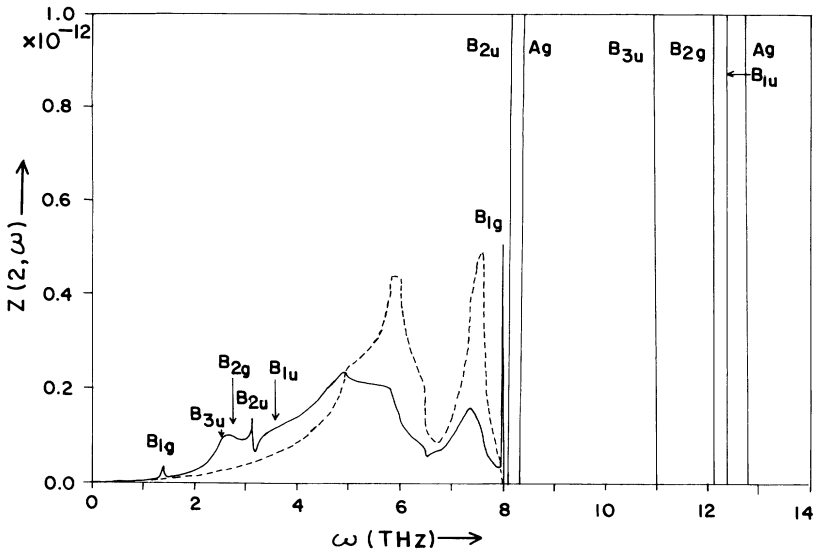

FIG. 4. Local density of vibrational states of atom 2 (——) and an atom in the host lattice (— — —).

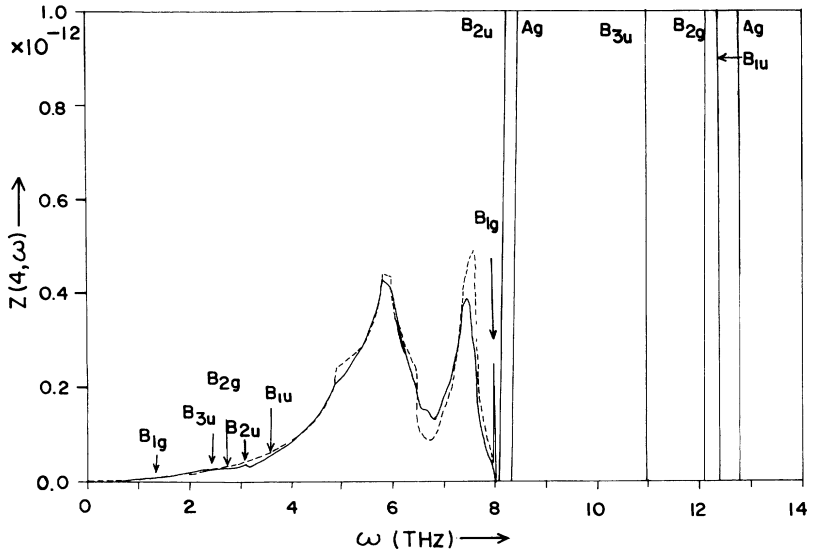

FIG. 5. Local density of vibrational states of atom 4 (——) and an atom in the host lattice (— — —).

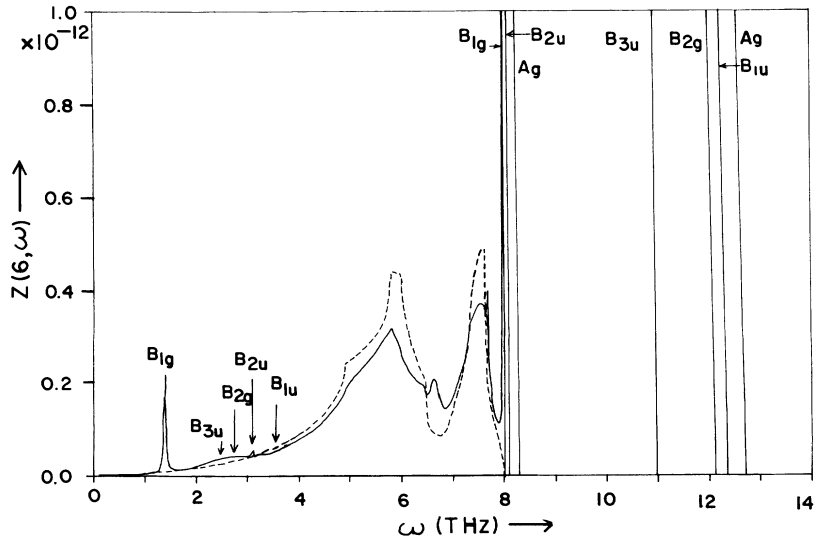

FIG. 6. Local density of vibrational states of atom 6 (——) and an atom in the host lattice (— — —).

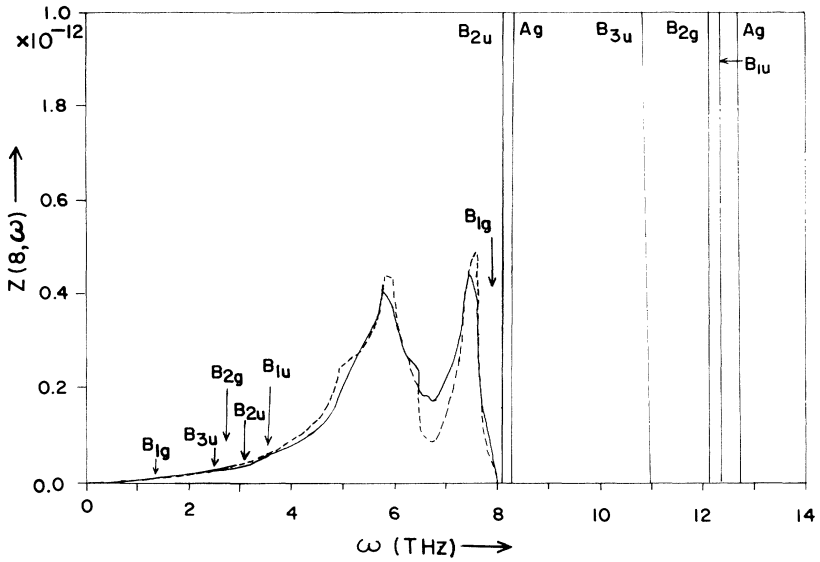

FIG. 7. Local density of vibrational states of atom 8 (——) and an atom in the host lattice (— — —).

tra have been calculated, the spectrum of atom 6 (Fig. 6) shows two sharp peaks pertaining to B_{1g} resonant modes (1.39 and 7.955 THz), while the intensities of all other resonant modes are so much reduced that except for a very small peak corresponding to the B_{2u} mode other resonant modes are hardly discernible. As might be expected, the motion of atom 6 in the (001) plane is strongly influenced by the dumbbell atom, and consequently modes in which the x and/or y components of its vibrations are involved should show significant amplitude of vibration while modes involving the z component of its motion are expected to be undetectable. Significantly, as is clear from Eqs. (9a) and (9b), all three resonant peaks (two B_{1g} and one B_{2u}) correspond to x and y components of the motion of this atom. The frequency spectrum of atom 4 shows only one resonant peak at 7.995 THz corresponding to the B_{1g} mode. Except for this the spectrum, more or less, resembles the host spectrum. The frequency spectrum of atom 8 does not show any resonant structure and is almost identical to the host spectrum. This result is not surprising: the more an atom is removed from the defect the more similar is its frequency spectrum to that of the host atom.

We have calculated the mean-square thermal displacement of different atoms using the calculated frequency spectra. The mean-square thermal displacement of an atom is

$$\langle u_\alpha^2(l)\rangle = \int \frac{Z_\alpha(l,l;\omega)}{2M\omega}\hbar\coth(\hbar\omega/2kT)d\omega\ , \qquad (14)$$

which becomes proportional to T at high temperatures,

$$\langle u_\alpha^2(l)\rangle = kTG_{\alpha\alpha}(l,l;\omega=0),\quad kT>\hbar\omega\ . \qquad (15)$$

The calculated mean-square thermal displacements for a dumbbell atom, atom 2, and a host atom are given in Fig. 8. For the other neighbors the mean-square thermal displacement is almost the same as that of the host atom. As can be seen from Fig. 8, while $\langle u^2\rangle$ for the dumbbell atom is strongly increased, that of atom 2 is almost like that of a host atom except for a slight increase above 100 K. Such a strong increase in $\langle u^2\rangle$ for the dumbbell is because of the sharp resonant modes at low frequencies. In fact, the thermal population of resonant modes connected

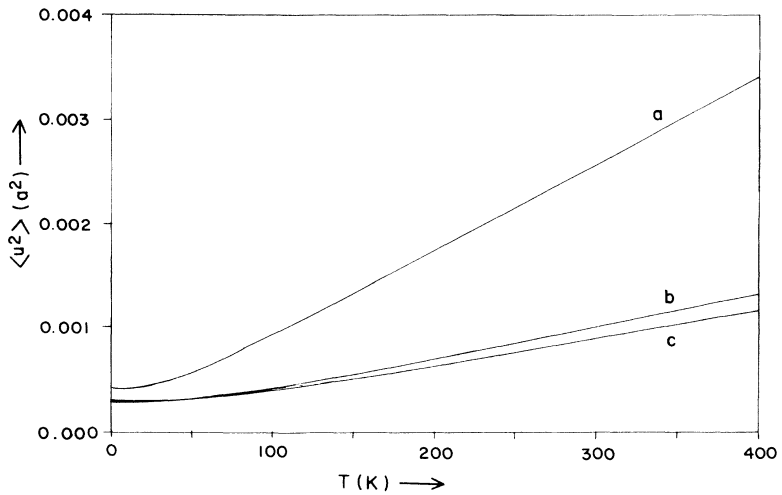

FIG. 8. Mean-square thermal displacement for the (a) dumbbell atom, (b) closest neighbor in the $(1\bar{1}0)$ plane, and (c) host atom.

with the interstitial diffusion stage I_D at 40 K is responsible for the strong increase of $\langle u^2 \rangle$.[16] A similar increase in $\langle u^2 \rangle$ for atom 2 is discernible at 40 K, but the contribution of resonant modes is not strong enough to cause significant increase. The slight increase in $\langle u^2 \rangle$ of atom 2 is attributed to its low amplitude of vibrations in the low-frequency resonant modes. The loss of modes from the high-frequency side of the spectrum with no corresponding gain in the low-frequency region is really responsible for this type of behavior, since the localized modes contribute little to the mean-square displacement because of the frequency factor in the denominator.

At this point a discussion of the present result in the light of the Mössbauer measurements of irradiated *Mo* ^{57}Co by Marangos, Mansel, and Wahl[15] seems to be in order. For a comparison with experiment the effect of the change in mass and possible force-constant changes on account of substitution of the host atom by the Mössbauer impurity ^{57}Co should be taken into account. However, in the context of the Debye-Waller factor, the effects of mass change and force-constant change are significant when the impurity gives rise to a low-frequency resonance mode. With Co being lighter than the host atom, a resonance mode of the substitutional impurity itself is not expected. In any case, in view of the strong perturbation around the dumbbell atom with very high force constants, the effect of possible force-constant changes and mass change due to the Mössbauer impurity seems to be of little consequence. We therefore feel that a consideration of the vibrational behavior of atom 2 is sufficient for the present discussion.

That we get low-frequency resonant modes and high-frequency localized modes in which both the dumbbell atom and its neighbors (atom 2) participate is in agreement with the Mössbauer measurements. However, the explanation for the observed strong reduction in the Debye-Waller factor of the Mössbauer impurity is not clear; while according to the suggestion of Marangos, Mansel, and Wahl the vibrational modes of the ^{57}Co atom at a substitutional site nearest to the dumbbell are responsible for the reduction in the Debye-Waller factor, the low amplitude of vibrations of atom 2 obtained in the resonant modes induced by the defect complex, a seemingly general feature of the defect-induced resonant modes,[23] makes such an explanation untenable. In fact, contrary to the expectation of Marangos, Mansel, and Wahl that there is a strong shift of the density of states of the Mössbauer atom to the lower frequencies, the spectrum of atom 2 shows a general shift of modes to lower as well as higher frequencies, with the amplitude of vibration being quite small in the low-frequency resonant modes. On the other hand, if we assume a mixed-dumbbell configuration for the defect complex it is more likely that the vibrational modes of the Mössbauer atom explain the reduction in the Debye-Waller factor. However, the ratio $\langle u^2 \rangle_{\text{dumbbell}} / \langle u^2 \rangle_{\text{host}}$ of the mean-square displacement amplitudes of the dumbbell atom and a host atom is not sufficiently high to account fully for the observed reduction in Debye-Waller factor; for example, at 80 K $\langle u^2 \rangle_{\text{dumbbell}} / \langle u^2 \rangle_{\text{host}}$ ($\simeq 2$) is one-third of the observed ratio $\langle u^2 \rangle_1 / \langle u^2 \rangle_{\text{sub}}$ ($\simeq 6$) of mean-square displacement amplitudes of a "trapper" ^{57}Co atom in the configuration of Fig. 1 and a ^{57}Co atom on a regular substitutional lattice site at the same temperature.[15] But then in the mixed-dumbbell configuration, caging and rotational motion of the mixed dumbbell are also possible. A planar caging motion of the solute atom is possible, giving rise to a reorientation of the dumbbell axis.[24] In any case, whether a caging motion of the solute atom, or its vibrational modes in the mixed-dumbbell configuration, is responsible for the strong reduction in the Debye-Waller factor is of interest only when the defect complex is assumed to be a mixed dumbbell. In view of the identification of the mixed-dumbbell configuration with a defect above 125 K by Marangos, Mansel, and Wahl,[15] the question of interpretation of the strong reduction in the Debye-Waller factor should be considered as yet open, and apparently more theoretical as well as experimental work is needed to clarify the situation.

ACKNOWLEDGMENTS

This work was supported by the Department of Science and Technology, India. One of us (S.S.P.) is grateful to the Council of Scientific and Industrial Research, New Delhi, for partial financial support. Part of the computation was done at the Computer Centre, NEHU, Shillong.

[1]P. N. Ram, Radiat. Eff. Defects Solids, **118**, 1 (1991).
[2]P. H. Dederichs, C. Lehmann, H. R. Schober, A. Scholz, and R. Zeller, J. Nucl. Mater. **69&70**, 176 (1978).
[3]P. H. Dederichs and R. Zeller, in *Point Defects in Metals II*, edited by G. Höhler and E. A. Niekisch, Springer Tracts in Modern Physics Vol. 87 (Springer, Berlin, 1980).
[4]W. Schilling, J. Nucl. Mater. **69&70**, 465 (1978).
[5]F. W. Young, Jr., J. Nucl. Mater. **69&70**, 310 (1978).
[6]P. H. Dederichs, C. Lehmann, and A. Scholz, Phys. Rev. Lett. **31**, 1130 (1973).
[7]H. R. Schober, V. K. Tewary, and P. H. Dederichs, Z. Phys. B **21**, 225 (1975); R. F. Wood and M. Mostoller, Phys. Rev. Lett. **35**, 45 (1975); P. N. Ram, J. Phys. F **15**, 35 (1985).
[8]R. Zeller and P. H. Dederichs, Z. Phys. B **25**, 139 (1976).
[9]P. N. Ram and P. H. Dederichs, Z. Phys. B **42**, 57 (1981).
[10]P. N. Ram, Phys. Rev. B **30**, 6146 (1984); **37**, 6783 (1988).
[11]P. H. Dederichs, C. Lehmann, and A. Scholz, Z. Phys. B **20**, 155 (1975).
[12]R. Urban, P. Ehrhart, W. Schilling, H. R. Schober, and H. Lauter, Mater. Sci. Forum **15-18**, 243 (1987); Phys. Status Solidi B **144**, 287 (1987).
[13]C. Erginsoy, G. H. Vineyard, and A. Englert, Phys. Rev. **133**, A595 (1964); R. A. Johnson, *ibid.* **134**, A1329 (1964); Y. Taji, T. Iwata, T. Yokata, and M. Fusse, Phys. Rev. B **39**, 6381 (1989); K. M. Miller, J. Phys. F **11**, 1175 (1981); N. W. Guinan, R. N. Stuart, and T. J. Borg, Phys. Rev. B **15**, 699 (1977).
[14]J. Marangos, W. Mansel, and G. Vogl, Radiat. Eff. **83**, 251 (1984).
[15]J. Marangos, W. Mansel, and D. Wahl, Mater. Sci. Forum

15-18, 255 (1987).
[16]P. N. Ram, Phys. Rev. B **43**, 6977 (1991).
[17]P. N. Ram, Phys. Rev. B **43**, 6480 (1991).
[18]A. D. B. Woods and S. H. Chen, Solid State Commun. **2**, 233 (1964).
[19]G. Gilat and L. J. Raubenheimer, Phys. Rev. **144**, 390 (1966).
[20]R. A. Johnson, and W. D. Wilson, in *Interatomic Potentials and Simulation of Lattice Defects,* edited by P. C. Gehlen, J. R. Beeler, Jr., and R. I. Jafee (Plenum, New York, 1972), p. 301.
[21]R. Weber, Ph.D. thesis, University of Freiburg, 1967.
[22]R. Zeller (unpublished).
[23]A. S. Barker, Jr., and A. J. Sievers, Rev. Mod. Phys. **47**, Suppl. **2**, S1 (1975).
[24]K. H. Robrock, Mater. Sci. Forum **15-18**, 5347 (1987).